Published in *Eur. Phys. J. - Spec. Topics* **185**, 181-193 (2010).

EPJ manuscript No.
(will be inserted by the editor)

Rogue waves in superfluid helium

V. B. Efimov[1,2,a], A. N. Ganshin[1,b], G. V. Kolmakov[1,3,c], P. V. E. McClintock[1,d], and L. P. Mezhov-Deglin[2,e]

[1] Department of Physics, Lancaster University, Lancaster, LA1 4YB, UK
[2] Institute of Solid State Physics RAS, Chernogolovka, Moscow region, 142432, Russia
[3] Department of Chemical and Petroleum Engineering, Pittsburgh University, Pittsburgh, PA 15261, USA.

Abstract. Rogue waves have been observed in superfluid helium. The experimental system consists of high intensity second sound (temperature-entropy) waves within a resonant cavity. Under steady state conditions, with a constant oscillatory driving force at the resonant frequency, the waves are turbulent and there are fluxes of energy towards both high and low frequencies. Rogue waves appear under the nonequilibrium conditions that prevail shortly after the drive has been switched on, prior to establishment of the steady state. The experiment is described briefly, relevant results are presented and discussed theoretically in terms of nonlinear wave interactions, and possible connections to rogue waves on the ocean are considered.

1 Introduction

Rogue waves have long been recognized by sailors as a menace to shipping and believed to be responsible for the unexplained losses of vessels of all sizes, including e.g. 22 super-carriers between 1968 and 1994 [1,2]. Rogue waves on the laboratory scale are in principle easier to investigate, and have now been been observed in a number of different systems, including superfluid ^{4}He [3] as we discuss below. In the rest of this introduction we summarize very briefly the notion of rogue waves in Sec. 1.1 and then in Sec. 1.2 we provide the basic information about superfluid ^{4}He needed to understand our recent experiments on rogue waves in second sound. The experiments themselves are described in Sec. 2 and discussed theoretically in Sec. 3. The results and the possible relationship of rogue waves in second sound to oceanic rogue waves are presented and considered in Sec. 4, and we draw conclusions in Sec. 5.

1.1 Rogue waves

Rogue waves on the ocean [2] are rare, and are much higher (and steeper) than all the other waves around them. They seem to appear from nowhere and subsequently to disappear without trace [4,5]. Following the famous "New Year wave" [6] measured by instruments on the Draupner North Sea oil rig at the beginning of 1995, the existence of oceanic rogue waves is no longer in doubt. On account of their interest and commercial importance, intensive research is in progress

[a] e-mail: efimov@issp.ac.ru
[b] e-mail: a.ganshyn@lancaster.ac.uk
[c] e-mail: gek11@pitt.edu
[d] e-mail: p.v.e.mcclintock@lancaster.ac.uk
[e] e-mail: mezhov@issp.ac.ru

to try to establish how rogue waves arise, in the hope that understanding may help in avoiding and possibly even controlling them.

There have been several suggestions about possible mechanisms for the creation of rogue waves. These include the combined effects of wind and currents, and the focusing effects associated with the profile of the ocean floor and nearby shorelines. Where rogue waves appear in deep water far from any shore, which they sometimes do, it seems likely that they must evolve through nonlinear interactions within the "noisy background" of smaller wind-blown waves [7]. Rogue waves have been modeled theoretically, especially by exploiting the special properties of the nonlinear Schrödinger equation [8,1,9,4,5]. They have been sought experimentally and/or studied in large wave tanks [10], optical systems [11,12], and superfluid ^{4}He [3]. Despite this growing body of work, extraordinarily little can be stated with confidence about the origins of rogue waves on the ocean. Open questions include:

1. Is the rogue wave phenomenon linear or nonlinear?
2. How do rogue waves appear? Is the phenomenon related to the modulation instability [13]?
3. What is the spectral content of rogue waves?
4. How important is the distribution of wave amplitudes in registering the rogue waves?
5. Can rogue waves be considered as classical large fluctuations [14–16]? In this context we comment that they might then be expected to possess deterministic features in the sense of developing and decaying along optimal paths, despite the inherently random, fluctuational, mechanisms that generate them.

In Sec. 5 we will return to these questions and consider the extent to which the present research illuminates them.

1.2 Superfluid helium

When cooled below 4.2 K under atmospheric pressure, ^{4}He condenses to form a colourless liquid that has many unusual features including, in particular, a density three times smaller than estimated for hard spheres the size of ^{4}He atoms in contact with each other [17]. The low density arises on account of the large quantum mechanical zero-point energy, combined with the very weak Van der Waals interatomic force: the liquid expands to minimise its free energy. The large interatomic separation endows the liquid with gas-like properties, so that it undergoes Bose-Einstein condensation [18] when cooled though a temperature $T = T_\lambda = 2.17\,\mathrm{K}$. Below T_λ, the properties of the liquid are so utterly different that it is called He II to distinguish it from He I above T_λ. Remarkably, He II behaves as though it were a mixture of two different fluids: a normal fluid component with viscosity and carrying all of the thermal energy of the liquid; and an inviscid superfluid component with zero entropy. The two fluids pass through each other without interaction: each of them separately fills the containing vessel. Oscillatory counterflow of the two components can occur at constant density and pressure, corresponding to the temperature-entropy wave known as *second sound*.

Second sound has a relatively low phase velocity ($\sim 20\,\mathrm{ms}^{-1}$) and an extremely small attenuation coefficient for frequencies below about 1 MHz. Its velocity u_2 depends strongly on its amplitude δT and can be approximated as

$$u_2 = u_{20}(1 + \alpha\delta T), \tag{1}$$

where u_{20} is the velocity at vanishingly small amplitude. The nonlinearity coefficient α [19] can be made large, and either positive or negative, by adjustment of the temperature. Because α determines the strength of the wave interactions, which can thus be easily controlled, these properties make He II an ideal medium for systematic studies of nonlinear interactions between waves.

2 Experiments on wave turbulence in second sound

The experiment involves studying second sound within a resonant cavity. Because of its small attenuation coefficient for frequencies below 1 MHz, the quality Q factor is typically $\sim$3000,

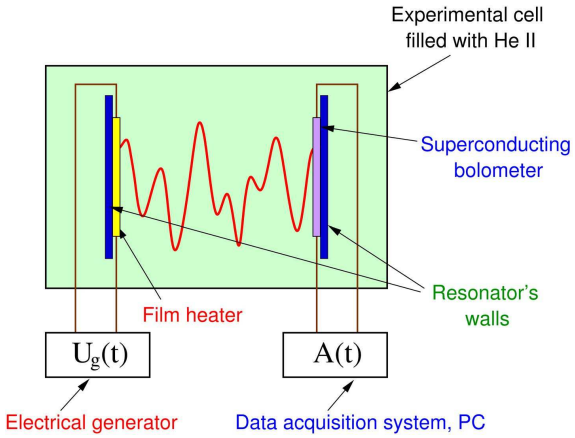

Fig. 1. Schematic diagram to illustrate the experimental arrangements.

enabling large wave amplitudes to be achieved without difficulty. These lead to nonlinear wave interactions and to the range of interesting phenomena that we describe below. First, we provide a brief account of how the experiments were performed.

2.1 Experimental details

Fig. 1 provides a schematic illustration of the experimental arrangements [20,21]. The resonator consists of a cylindrical quartz tube of length $L = 7$ cm and inner diameter $D = 1.5$ cm, filled with superfluid helium. Being a temperature wave, second sound can conveniently be excited with a heater and detected thermometrically. Accordingly, a thin-film heater and bolometer were deposited on the surfaces of flat glass plates capping the ends of the tube. The heater was driven by a harmonic voltage generator in the frequency range 0.1 – 100 kHz. The frequency of the second sound (twice the frequency of the voltage generator) was set close to a longitudinal resonance. The amplitude δT of the standing wave could be varied between 0.05 mK and a few mK. The temperature was maintained at $T \approx 2.08$ K, for which $\alpha \approx -7.7$ K^{-1}. The resonator's Q-factor, determined from the widths of longitudinal resonances at small heat flux densities (linear regime), was $Q \sim 3000$ for resonance numbers $30 < n < 100$. The second sound wave shape detected by the bolometer was recorded as a time series, and its power spectrum was subsequently computed by fast Fourier transform (FFT).

2.2 Results under steady state conditions

Fig. 2(a) shows typical steady state results under experimental conditions such that only the direct cascade exists. Energy injected at the driving frequency flows steadily towards higher frequencies with negligible dissipation until the viscous cut-off is reached, beyond which it is rapidly dissipated as heat. Fig. 2(b) shows the very different situation that applies under conditions such that the inverse and direct cascades coexist. The energy flux from the drive is then shared between the two cascades. As before, some energy flows towards higher frequencies, but half or more of it flows towards lower frequencies. It is believed that energy flowing in the latter (inverse) cascade is eventually dissipated by normal fluid damping on the resonator walls.

The inverse cascade appears quite suddenly as the amplitude is increased or the detuning of the drive from the resonant frequency is decreased, and it appears to be associated with an instability against the formation of subharmonics. To characterise the instability quantitatively, we use the energy contained in the low-frequency part of the spectrum $\omega < \omega_d$,

$$E_{LF} = \frac{1}{2}\left(\frac{\partial C}{\partial T}\right) \sum_{\omega<\omega_d} |\delta T_\omega|^2, \tag{2}$$

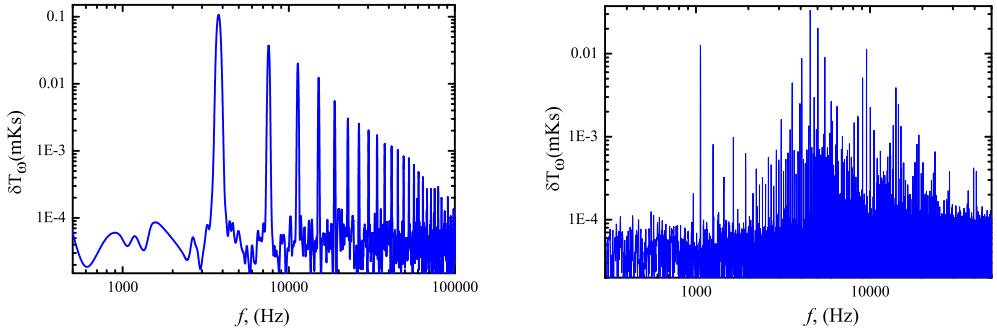

Fig. 2. Steady state power spectral amplitudes δT_ω of standing waves in the resonant cavity, for $T = 2.079\,\mathrm{K}$. Left: direct energy cascade when driving close to the 37th resonant frequency, $f_d = 3780\,\mathrm{Hz}$. The ac heat flux density from the heater was $W = 30\,\mathrm{mW/cm^2}$. Right: coexistence of the inverse and direct energy cascades for the 96th resonance with $W = 19.2\,\mathrm{mW/cm^2}$.

as an indicator. Here C is the heat capacity per unit volume. For small W with fixed detuning, we did not observe any subharmonic generation at all [20]; then, above a critical flux W_c, E_{LF} rose rapidly [3], as shown in Fig. 3. This critical character of the phenomenon is fully in accord with theoretical expectations (see below and [3]. At $T = T_\alpha = 1.88$ K for which α vanishes [19], no subharmonics were observed, regardless of the magnitude of W, thus confirming the crucial importance of nonlinearity. These phenomena appear in the regime where the energy cascade towards the high frequency domain (i.e. direct cascade, with a Kolmogorov-like spectrum [20, 22]), is already well-developed. We have found that they are attributable mainly to 3-wave interactions, i.e. to a decay instability whereby the wave decays into two waves of lower frequency governed by the energy (frequency) conservation law

$$\omega_1 = \omega_2 + \omega_3 \tag{3}$$

where $\omega_i = u_{20} k_i$ is the frequency of a linear wave of wave vector k_i. The inverse process is, of course, also possible.

2.3 Results in transient evolution and rogue waves

The results shown in Fig. 2 were recorded after leaving the system for a few minutes to reach its steady state for any give parameter set. It of particular interest, however, to observe the transient evolution of the system after the drive is switched on or off, or after a parameter is changed. Fig. 4 presents typical results obtained when driving at a relatively high resonant frequency ω_d (the 96th longitudinal resonance of the cell). Fig. 4(a) plots the measured second sound signal after switching on the drive at $t \sim 0.4\,\mathrm{s}$. Figs. 4(b) shows an expanded window just after switch-on and (c) shows its power spectrum. These data are similar to those for the direct Kolmogorov-like cascade under steady state conditions (Fig. 2(a) [20]), when driving close to resonance. Thus it can be seen that the direct cascade appears almost immediately after switch-on. Figs. 2(f),(g) provide comparable plots for window-3, where it is evident that the results are approaching those for the steady state when the inverse cascade is active (Fig. 2(b)).

Of particular interest in the present context are the results of Fig. 4(a) in the intermediate range. A sequence of rogue waves is clearly evident; (d) plots an expansion of the one seen in window-2, and (e) gives its power spectrum. So far, we have only observed rogue waves under transient conditions like those illustrated, during the development of the inverse energy cascade.

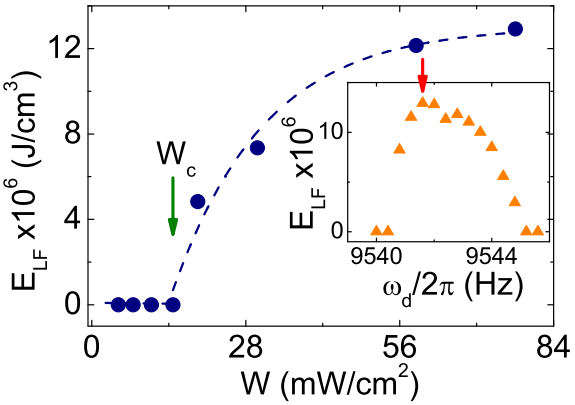

Fig. 3. The energy E_{LF} contained in the low-frequency part of the spectrum as a function of the AC heat flux density W, while driving near to the 96th resonance for $T \simeq 2.08$ K. The threshold value of W, marked by the (green) arrow, was $W_c = 10.4$ mW/cm^2. The points are from experiment; dashed lines are guides to the eye. Inset: the dependence of E_{LF} on ω_d, measured for $W = 55.6$ mW/cm^2; the (red) arrow labels the maximum value of E_{LF}, which is taken to the main figure. From [3]

3 Theoretical considerations

In seeking to understand the peculiarities of this transient process we have undertaken analytical and numerical studies of the dynamics of the nonlinear wave system. Full details of the techniques have been given elsewhere [23,20] but, in essence, it involves direct integration of the two-fluid hydrodynamical equations, expanded up to quadratic terms in the wave amplitude. We use a representation of the second sound waves in the resonator in term of Hamiltonian variables [23], a numerical technique somewhat similar to that used in [7]. It allows one to capture accurately the shape of the wave at large amplitudes and/or gradients [8]. The equation of motion governing energy balance in the system is

$$i\frac{\partial b_n}{\partial t} = \sum_{n_1,n_2} V_{n,n_1,n_2}(b_{n_1}b_{n_2}\delta_{n-n_1-n_2} + 2b_{n_1}b^*_{n_2}\delta_{n_1-n_2-n}) - i\gamma_n b_n + F, \qquad (4)$$

where $b_n(t) = (1/2)(B_n^{-1}S_n + iB_n\beta_n)$ is the time-dependent canonical amplitude of second sound at the n-th resonant frequency f_n; S_n and β_n are the space Fourier components $\sim \cos(2\pi f_n x/u_{20}L)$ of the entropy and of the potential of the normal-superfluid relative velocity; $B_n = (f_nC/T)^{1/2}$; $V_{n,n_1,n_2} \propto \alpha(nn_1n_2)^{1/2}$ describes the three-wave interaction; $\gamma_n = \nu n^2$ models the viscous damping of second sound; and $F \propto W$ is the amplitude of the force driving the n-th resonant mode. In this representation the wave spectrum can be calculated as $A_f \propto B_n\,(b_n + b^*_n)$.

3.1 Generation of low frequency waves near the instability threshold

First, we consider generation of low-frequency harmonics due to nonlinearity of the second sound wave. It is known that the problem of nonlinear wave propagation and interaction can be mapped onto the problem of coupled oscillator dynamics (see [24] for general formalism and [25,23] for application to second sound in ^{4}He). Based on quite general considerations [26], we may expect the production of waves in the low-frequency domain to be initiated at a frequency close to half that at which the energy is being injected into the system. Accordingly, to establish conditions for the wave instability, we consider a simplified problem where just two interacting

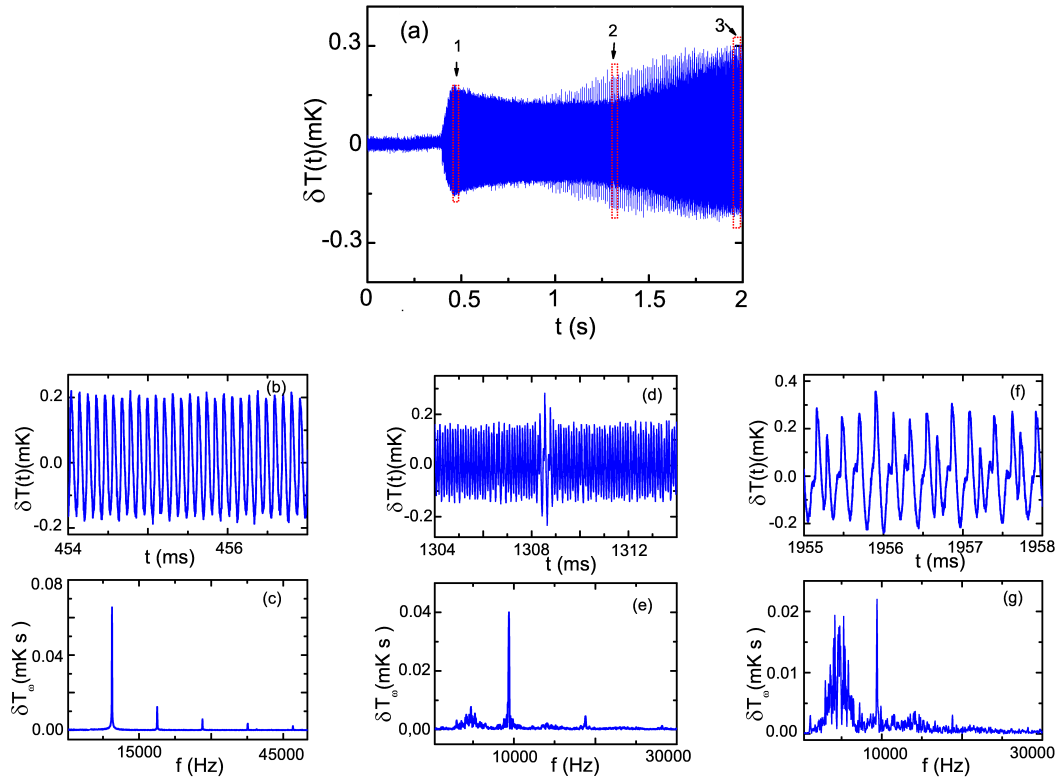

Fig. 4. (a) Transient evolution of the second sound wave system after switching on the drive at a frequency near the 96th resonance. The AC heat flux density was $W = 42.1$ mW/cm^2. The signals (b),(d),(f) and instantaneous spectra (c),(e),(g) correspond to the time windows indicated in (a) by the arrows 1-3 respectively. Note the linear ordinate scales in (c),(e),(g) (cf. the logarithmic ordinates in Fig. 2).

wave modes at $\omega = \omega_d$ and $\omega = \omega_d/2$ are taken into account. In this case the model Hamiltonian of the system reads

$$H = \omega_1 |b_1|^2 + \omega_2 |b_2|^2 + \lambda b_1^2 b_2^* + \lambda b_1^{*2} b_2. \tag{5}$$

Here ω_1 and ω_2 are the resonant frequencies of second sound waves of infinitely small amplitude, b_1 and b_2 are normal coordinates (below we will call them the amplitudes of second sound waves), λ is the amplitude of the three-wave interactions proportional to the nonlinearity coefficient of second sound. The two terms cubic in the wave amplitude describe the interaction of waves due to nonlinearity [27]. The subscript "1" labels the wave of lower frequency (the low-frequency, or LF wave), and subscript "2" labels the wave of higher frequency (the high frequency or HF wave), i.e. $\omega_1 < \omega_2$. We assume also that the external driving force is applied at a frequency close to the frequency ω_2.

The equations of motion for the amplitudes of weakly dissipating second sound waves are [24,25]

$$i\dot{b}_1 = \frac{\partial H}{\partial b_1^*} - i\gamma_1 b_1, \qquad i\dot{b}_2 = \frac{\partial H}{\partial b_2^*} - i\gamma_2 b_2 + F(t), \tag{6}$$

where γ_1 and γ_2 are the damping coefficients of second sound waves, and $F(t)$ is a monochromatic driving force applied at a frequency ω,

$$F(t) = F \exp(-i\omega_d t),$$

F is the time-independent driving amplitude, and the dot denotes a derivative with respect to time t. For further analysis it is convenient to use an interaction representation for the wave

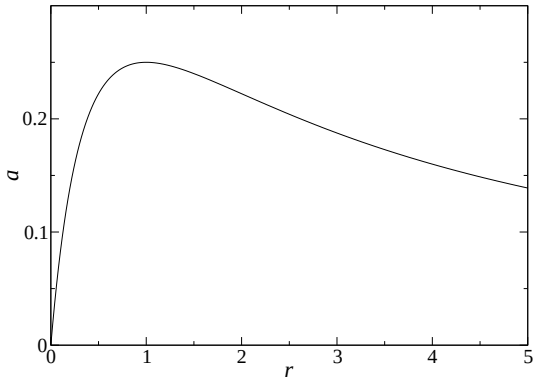

Fig. 5. Dependence of the a parameter on the ratio $r = Q_1/Q_2$ of the quality factors at the frequencies of the LF and HF second sound waves.

amplitudes,

$$b_1 = A_1 \exp(-i\omega_d t/2), \quad b_2 = A_2 \exp(-i\omega_d t) \tag{7}$$

where A_1 and A_2 are new variables. In steady state, A_1 and A_2 are time-independent. In this case the equations (6) read

$$0 = i\dot{A}_1 = -\frac{1}{2}(\Delta\omega + 2i\gamma_1)A_1 + 2\lambda A_1^* A_2, \tag{8}$$

$$0 = i\dot{A}_2 = -(\Delta\omega + i\gamma_2)A_2 + \lambda A_1^2 + F. \tag{9}$$

Here $\Delta\omega = \omega_d - \omega_2$ is the detuning of the driving force with respect to the resonance frequency of the HF wave.

The amplitude of the HF wave can be eliminated from the set of equations (8), (9). The resulting equation for the amplitude of the LF wave in steady-state reads

$$(\Delta\omega^2 - 2\gamma_1\gamma_2 - 4\lambda^2|A_1|^2)^2 + \Delta\omega^2(\gamma_1 + 2\gamma_2)^2 = 16\lambda^2|F|^2 \tag{10}$$

For convenience, we now introduce dimensionless variables for the wave amplitude, driving force, detuning, and damping:

$$\xi_1 = \frac{2\lambda|A_1|}{\gamma_2 + 2\gamma_1}, \quad f = \frac{4\lambda|F|}{(\gamma_2 + 2\gamma_1)^2}, \quad \Delta = \frac{\omega - \omega_2}{\gamma_2 + 2\gamma_1}, \quad a = \frac{2\gamma_1\gamma_2}{(\gamma_2 + 2\gamma_1)^2}. \tag{11}$$

In terms of these dimensionless variables, equation (10) becomes

$$\xi_1 = \left[(f^2 - \Delta^2)^{1/2} + \Delta^2 - a\right]^{1/2} \tag{12}$$

The parameter a is expressed in terms of the quality factor of the resonator $Q_1 = \omega_1/\gamma_1$ and $Q_2 = \omega_2/\gamma_2$ at frequencies equal to the frequencies of LF and HF waves, as follows

$$a = \frac{Q_1 Q_2}{(Q_1 + Q_2)^2}$$

The dependence of the $a(r)$ parameter on the ratio $r = Q_1/Q_2$ is shown in Fig. 5. It has a maximum $a = 1/4$ at $r = 1$. Assuming the dependence on frequency of the damping coefficient for second sound takes the form $\gamma(\omega) = \nu_0\omega^2$, which is typical for sound waves in an unrestricted liquid, we may evaluate the a coefficient as (recall here that $\omega_1 \approx \omega_2/2$)

$$\gamma_1/\gamma_2 = 0.25, \quad a \approx 0.2$$

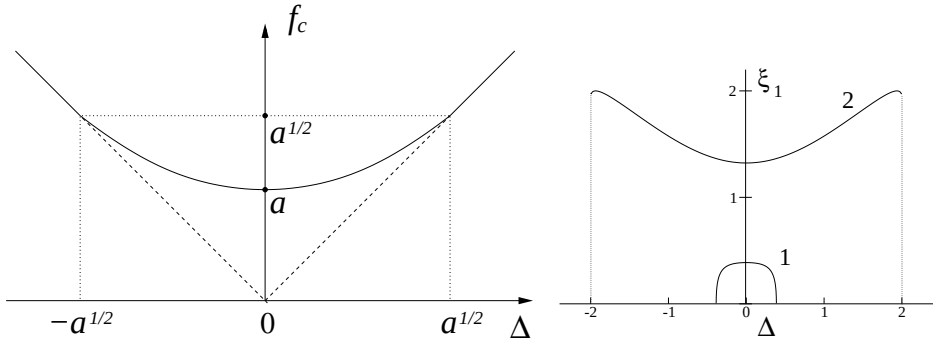

Fig. 6. Left: calculated dependence of the critical amplitude of the driving force on the detuning Δ from the second sound resonant frequency. Right: amplitude of the LF wave plotted as a function of detuning for two driving amplitudes, $f = 0.4$ (i.e. $f < a^{1/2}$, curve 1), and $f = 2$ ($f > a^{1/2}$, curve 2). The damping is $a = 1/4$.

that is close to its maximum value. It follows from Eq. (12) that the amplitude of the LF wave is nonzero only if the amplitude of the driving force at the frequency of the HF wave exceeds a critical value $f_c = \max(f_{c1}, f_{c2})$, and if f_{c1} and f_{c2} obey the following conditions:

$$f_{c1} - |\Delta| = 0, \tag{13}$$

$$(f_{c2}^2 - \Delta^2)^{1/2} + \Delta^2 - a = 0. \tag{14}$$

The dependence of the critical amplitude of the driving force f_c on the detuning Δ defined by (13) and (14) is shown in Fig. 6(left).

It follows from subsequent analysis that, in the area inside the rectangle ($\Delta| < a^{1/2}$, $a < f < a^{1/2}$) in Fig. 6(left), the generation of the LF wave is somewhat similar to a second order transition, because the amplitude ξ_1 starts from zero. At $f > a^{1/2}$ the generation of the LF frequency is of the hard type, however, analogous to a first order transition, and it is accompanied by a finite jump in wave amplitude.

To demonstrate this, let us consider the dependence of the amplitude of the LF wave ξ_1 on the detuning Δ for a given value of the driving force f. At $f \le f_{c\,min} = a$ the amplitude ξ_1 is equal to zero. At $f > f_{c\,min}$ there are two possibilities: in accordance with Eq. (12) the second derivative the amplitude ξ_1 with respect to Δ taken at $\Delta = 0$,

$$\left.\frac{d^2\xi_1}{d\Delta^2}\right|_{\Delta=0} = \frac{1-2f}{2f(f-a)^{1/2}.} \tag{15}$$

If $a < f < a^{1/2}$, the second derivative (15) is negative, and the amplitude ξ_2 at half the driving frequency decreases with increasing Δ (curve 1 in the right plot of Fig. 6). Recall that a is always less than unity. For the case $f > a^{1/2}$ the wave amplitude ξ_2 rises with an increase in the detuning (curve 2).

To estimate the critical wave amplitude above which generation of the low-frequency wave becomes possible, we take $\xi_1 \sim 1$, and [27]

$$\lambda = \sqrt{\frac{\rho_s}{\rho\rho_n}}\frac{\alpha\sigma\omega^{3/2}}{6\sqrt{2}u_2(\partial\sigma/\partial T)}, \quad \delta T = \sqrt{\frac{\omega}{(\partial S/\partial T)}}|A|, \quad |A| = \frac{(\gamma_2+2\gamma_1)}{2\lambda}\xi_1, \quad u_2^2 = \frac{\rho_s\sigma^2}{\rho_n(\partial\sigma/\partial T)} \tag{16}$$

From here one can estimate the critical second sound wave amplitude as $\delta T \sim \gamma/|\alpha|\omega = 1/|\alpha|Q$ where γ is the damping coefficient of the second sound wave, and Q is the quality factor of the resonator. Taking the values $Q \sim 10^3$, $|\alpha| \sim 7.7K^{-1}$ one has $\delta T \sim 0.1 \times 10^{-3}$K by order of magnitude, consistent with the experimental observations.

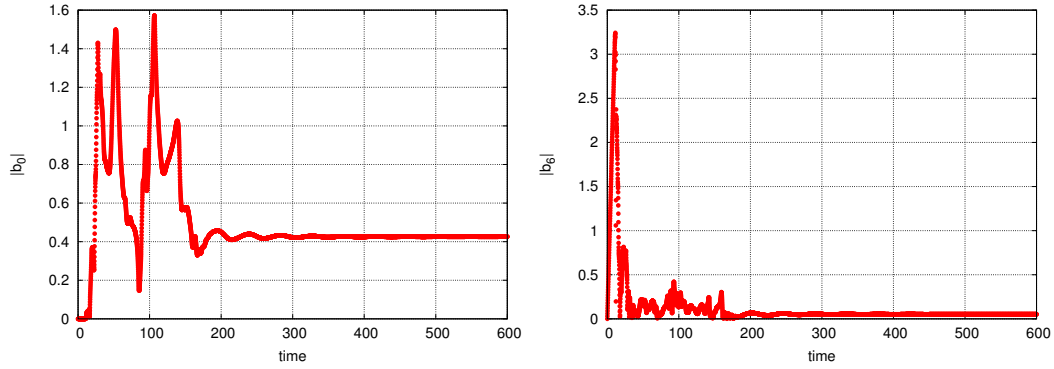

Fig. 7. Calculated evolution with time of the second sound wave amplitudes at the 1st (left) and 6th (right) resonant frequencies. The driving force is being applied at the 6th resonant frequency.

3.2 Numerical simulations

If the driving force amplitude exceeds the critical value for generation of low frequency waves (the region above the full curve in Fig. 6 left) multiple waves with $\omega < \omega_d$ may be excited as the result of nonlinearity. At high driving amplitudes the dynamics cannot be reduced to a simple model (5), and the full set of equations (4) must be considered. In this case, the nonlinear dynamics of the wave system is complicated and must be analyzed numerically. To capture the main characteristic features of the development of the inverse cascade while, at the same time, keeping the system simple enough to be analyzed in detail, we carry out a simulation within the framework of equations (4) taking account of relatively small numbers of waves N: the summation in Eq. (4) was made for n_1, n_2 ranging from 1 to N. In what follows we present the results obtained for $N = 10$. We assume that a periodic driving force is applied to the 6th resonant frequency.

It is important to note that, in accordance with Sec. 3.1, the inverse cascade develops as the result of instabilities in the wave at the driving frequency and in its harmonics. At small time, the dependence of the low frequency harmonic amplitudes on time is close to $b_n(t) \propto b_n(0)\exp(\nu_n t)$, where ν_n is the instability increment. If the initial conditions are set to $b_n(0) = 0$, the amplitudes will be kept formally equal to zero at any time $t > 0$. In simulations with zero initial conditions, the instability can be strongly affected by "numerical noise" due to discretization in the computational scheme. To avoid any such influence and resultant numerical artifacts, we apply non-zero initial conditions in our simulations for wave amplitudes at frequencies below the driving frequency. That is, we set the initial wave amplitudes to a very small non-zero value, $b_n(0) = b_0$; for the results reported here we took $b_0 = 10^{-4}$. We also checked that neither the details of the transient process, nor the final steady-state wave spectrum, depend on b_0 provided that b_0 is taken to be sufficiently small with respect to steady-state wave amplitudes measured at large time.

Fig. 7 shows the time dependence of the wave amplitudes at the 1st and 6th (driving) resonant frequencies. It is clearly evident that a low frequency wave is generated at $n = 1$ as the result of nonlinear interactions in the system. We checked in the computations that if we set the nonlinearity coefficient V_{n,n_1,n_2} to zero, waves with frequencies below the driving frequency are not then excited. Fig. 7 shows that the transient process extends over a relatively long time ($t \sim 200$ in numerical units), that is, a time much longer than the characteristic nonlinear time (~ 1) of this system. Fig. 8 demonstrates the steady-state wave spectrum computed for $t = 1000$. The driving frequency is marked by an arrow. It is evident that, in the low-frequency spectral domain, the wave amplitude rises with decreasing resonance number n, in accordance with experimental observations (Sec.2).

Fig. 9 shows the dependence on time of the wave amplitude computed at the edge of the resonator $\delta T(t, x = 0)$ (corresponding to the bolometer signal in our experiments). It can be seen that, at relatively small times (left plot) after the driving force was switched on, the signal

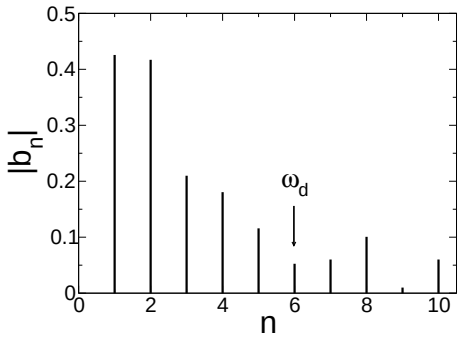

Fig. 8. Steady state second sound wave spectrum computed for $t = 1000$. The arrow indicates the frequency ω_d of the driving force.

presents a series of "freak waves" of amplitude more than twice that of the surrounding waves. At large times, $t \sim 300$, where the system is close to its steady state, the signal oscillates strongly at a low frequency which, again, is in qualitative agreement with experimental observations, Fig. 4(f).

4 Discussion

It is evident that the theory provides a good qualitative description of the phenomena seen in the experiments. How might these results be related to the appearance of rogue waves on the ocean? We will first discuss this question explicitly, then consider more generally whether rogue waves can usefully be considered as classical large fluctuations and whether this perception may help in their analysis, and finally return to the open questions listed in Sec. 1.1.

4.1 Rogue waves on the ocean and in superfluid ^{4}He

There are differences as well as similarities between rogue waves on the ocean and in superfluid ^{4}He. The similarities include –

1. In both cases, the phenomena under consideration are non-equilibrium in nature. Energy is continuously injected into the system, as entropy variations in the case of second sound and by e.g. wind and tide in the cases of ocean waves. In both cases the energy is eventually dissipated as heat.

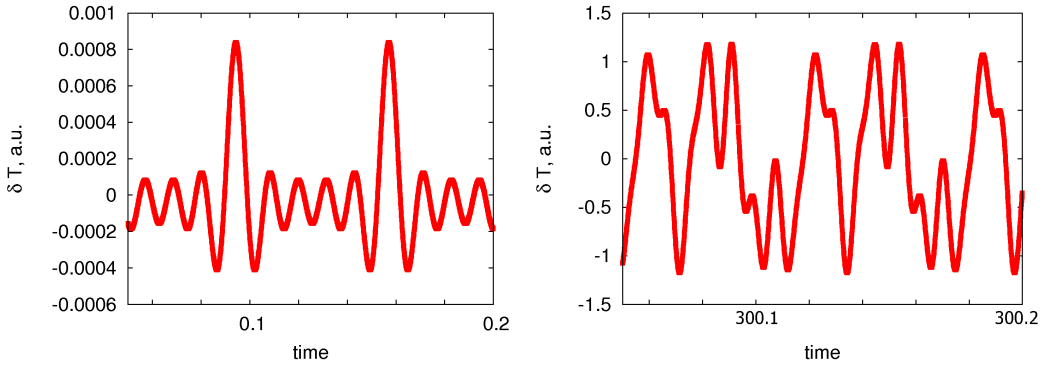

Fig. 9. Time dependence of the second sound wave amplitude computed at the edge of the resonator for small, $t \sim 0.1$ (left), and large, $t \sim 300$ (right), times after the moment when the driving force was switched on. Note the creation of rogue waves at early time.

2. In both cases, the rogue waves are rare, extreme, events – albeit less rare in the ^{4}He case where the rogue waves appear at first singly, but then in small groups that become progressively larger as the inverse cascade develops (not shown in Fig. 4). Of course, this might no longer be the case if we could identify steady state conditions for rogue waves in second sound but, at present, the possibility remains an open question.
3. In both cases, the phenomena appear to arise from an instability of large amplitude waves: a decay instability in the case of second sound, and (probably) a modulation instability of the ocean waves.

The differences include –

1. The second sound waves in the experiment are produced directly by a periodic driving force, whereas on the ocean roughly periodic waves are created by e.g. wind of a sufficient velocity.
2. The second sound waves are one-dimensional standing waves, within the volume of the fluid, whereas the ocean waves are on the surface and can propagate in two dimensions.
3. Rogue waves on the ocean can apparently appear under steady state conditions, whereas those in second sound have so far only been observed during the interval while the inverse energy cascade is evolving after switching on the drive and after establishment of the direct cascade.

4.2 Rogue waves as classical large fluctuations

Taken at face value, rogue waves look just like what physicists working on stochastic dynamics refer to as *large fluctuations*; mathematicians call them *large deviations*. The subject has a long history. The importance of large fluctuations seems first to have been recognized by Boltzmann [28] who introduced the concept in his 1904 speech in St Louis. Later, the idea was taken up and substantially developed by Onsager and Machlup [14] who introduced the notion of optimal fluctuational paths along which the system fluctuates with overwhelming probability when a large fluctuation occurs. Many theorists contributed to the further development of the idea, usually assuming the limit of vanishingly small noise intensity, which of course is not what pertains in real physical systems. There was little connection to reality until the appropriate statistical quantity, the *prehistory probability distribution*, had been introduced [15]. Only then could it be appreciated that, in a real system with finite fluctuation intensity, the optimal path corresponds to the ridge (locus of maxima) along the top of the prehistory distribution. This opened the way for experimental demonstrations [16, 29] of the time-reversal symmetry of large fluctuations in equilibrium systems, and their asymmetry in nonequilibrium systems, confirming Onsager and Machlup's earlier prescient ideas [14].

Given that the wave energy per unit area changes relatively slowly compared to the characteristic times associated with individual waves, it seems reasonable to suppose that the ocean can be regarded in this context as a quasi-equilibrium system. Consequently, one might hypothesize that the evolution and decay of rogue waves follow identical but time-reversed optimal paths. At least for numerical simulations, therefore, and possibly also for very large wave tanks, it may be possible to infer the evolutionary process by studying the decay of an artificially created rogue wave: the optimal path during evolution should simply be the time-reversed decay. It may also prove possible to map out the prehistory probability distribution of the rogue waves that we have observed in second sound, and we hope to attempt this project in the future.

Of course, viewing rogue waves as classical large fluctuations cannot by itself provide an adequate explanation because they appear too frequently. In this picture, one would have to invoke nonlinearity and specific mechanisms, e.g. of the kind described above, to account for the clearly non-Gaussian tails of the wave amplitude distribution. Nonetheless it may prove useful to bear this more general scenario in mind while considering detailed transformation mechanisms for the wave energy.

4.3 Origins of rogue waves

We can now return to the open questions posed in Sec. 1.1. In the light of the experiments and numerical simulations, and treating second sound acoustic turbulence as a model of what may happen on the ocean surface, we suggest that rogue waves are a nonlinear phenomenon that arises through the modulation instability (analogous to the decay instability in superfluid helium). The present experiments reveal immediately the spectral content of a wave system that includes rogue waves (Fig. 4(e)): we can of course select windows of different size in Fig. 4(a) to facilitate extraction of whatever spectral information is needed. The distribution of wave amplitudes in our measurements away from the rogue waves would seemingly not tell us that a rogue wave was imminent: the rogues are quite distinct from neighbouring waves and do not seem to have any precursors. Finally, regardless of the details of the production mechanism, rogue waves clearly have much in common with classical large fluctuations and this perception of rogue waves is likely to be worth pursuing.

5 Conclusion

Second sound in superfluid ^{4}He constitutes a convenient laboratory-scale experimental system for studies of rogue waves. We have shown through experimental observations and numerical simulation that it is the nonlinear interaction between the waves that is responsible for generation of the direct and inverse cascade in the wave system. Multiple freak waves were found to be created during the transient process towards the state where the inverse cascade exists in steady state. We suggest that the underlying mechanism for the development of the freak waves in superfluid helium, i.e. the decay instability of large amplitude waves, is similar to that responsible for the generation of huge waves on the ocean surface.

Acknowledgements

We acknowledge valuable discussions with Mark Dykman, Evgenii Kuznetsov, Alexandr Levchenko and Vladimir Zakharov. The work was supported by the Engineering and Physical Sciences Research Council (UK), by the Royal Society of London, by the Presidium of the Russian Academy of Sciences, and by the Russian Foundation for Basic Research.

References

1. C. Kharif, E. Pelinovsky, Eur. J. Mech. B/Fluids **22**, 603 (2003)
2. E.N. Pelinovsky, A. Slunyaev, A. Slunyaev, *Rogue Waves in the Ocean* (Springer-Verlag, Berlin, 2008)
3. A.N. Ganshin, V.B. Efimov, G.V. Kolmakov, L.P. Mezhov-Deglin, P.V.E. McClintock, Phys. Rev. Lett. **101**(6), 065303 (2008)
4. N. Akhmediev, A. Ankiewicz, M. Taki, Phys. Lett. A **373**, 675 (2009)
5. N. Akhmediev, J.M. Soto-Crespo, A. Ankiewicz, Phys. Lett. A **373**, 2137 (2009)
6. S. Haver, O.J. Andersen, *Freak waves: Rare realizations of a typical population or typical realizations of a rare population?*, in *Proc. 10th Intern. Offshore and Polar Engineering Conf.*, edited by J.S. Chung, R.M.W. Frederking, H. Saeki, W. Koterayama (ISOPE, Cupertino, CA, 2000), Vol. III, pp. 123–130
7. A.I. Dyachenko, V.E. Zakharov, JETP Lett. **81**, 255 (2005)
8. V.E. Zakharov, J. Appl. Mech. Tech. Phys. **9**(2), 190 (1968)
9. N. Akhmediev, J.M. Soto-Crespo, A. Ankiewicz, Phys. Rev. A **80**, 043818 (2009)
10. M. Onorato, T. Waseda, A. Toffoli, L. Cavaleri, O. Gramstad, P.A.E.M. Janssen, T. Kinoshita, J. Monbaliu, N. Mori, A.R. Osborne et al., Phys. Rev. Lett. **102**(11), 114502 (2009)
11. D.R. Solli, C. Ropers, P. Koonath, B. Jalali, Nature **450**(06402), 1054 (2007)
12. A. Montina, U. Bortolozzo, S. Residori, F.T. Arecchi, Phys. Rev. Lett. **103**, 173901 (2009)

13. D.H. Peregrine, J. Austral. Math. Soc. Ser. B **25**, 16 (1983)
14. L. Onsager, S. Machlup, Phys. Rev. **91**(6), 1505 (1953)
15. M.I. Dykman, P.V.E. McClintock, V.N. Smelyanskiy, N.D. Stein, N.G. Stocks, Phys. Rev. Let. **68**(18), 2718 (1992)
16. D.G. Luchinsky, P.V.E. McClintock, Nature **389**(6650), 463 (1997)
17. J. Wilks, *The Properties of Liquid and Solid Helium* (Clarendon Press, Oxford, 1967)
18. F. London, Nature **141**, 643 (1938)
19. A.J. Dessler, W.H. Fairbank, Phys. Rev. **104**, 6 (1956)
20. G.V. Kolmakov, V.B. Efimov, A.N. Ganshin, P.V.E. McClintock, L.P. Mezhov-Deglin, Phys. Rev. Lett. **97**, 155301 (2006)
21. V.B. Efimov, A.N. Ganshin, P.V.E. McClintock, G.V. Kolmakov, L.P. Mezhov-Deglin, J. Low Temp. Phys. **145**, 155 (2006)
22. G. Falkovich, M. Meyer, Phys. Rev. E **54**, 4431 (1996)
23. M.Y. Brazhnikov, V.B. Efimov, G.V. Kolmakov, A.A. Levchanko, E.V. Lebedeva, L.P. Mezhov-Deglin, Low Temp. Phys. **30**(6), 441 (2004)
24. V.E. Zakharov, V.S. L'vov, G. Falkovich, *Kolmogorov Spectra of Turbulence I* (Springer, Berlin, 1992)
25. V.L. Pokrovskii, I.M. Khalatnikov, Sov. Phys. JETP **44**, 1036 (1976)
26. V.S. L'vov, V.B. Cherepanov, Sov. Phys. JETP **54**, 746 (1982)
27. G.V. Kolmakov, Low Temp. Phys. **29**(6), 495 (2003)
28. L. Boltzmann, in *Theoretical Physics and Philosophical Problems*, edited by B. McGuinness (Reidel, Dordrecht, 1974), p. 15972
29. D.G. Luchinsky, P.V.E. McClintock, M.I. Dykman, Rep. Prog. Phys. **61**(8), 889 (1998)